by the Adaptable and Seamless Technology Transfer Program Through Target-Driven R&D from the Japan Society and Technology Agency (AS2421276Q); and by research project grants from Kawasaki Medical School (23-T1, 26-T1). The sponsors played no role in study design; in the collection, analysis, and interpretation of data; in the writing of the report; or in the decision to submit the article for publication.

Competing Interests: The authors have declared that no competing interests exist.

the ligand, but also prevents two distinct membrane receptors from binding to the ligand. This study provides a strong rationale for the use of p29 in the amelioration of skeletal muscle atrophy in various clinical settings.

Introduction

Myostatin, a muscle-specific transforming growth factor-β (TGF-β) family member, plays crucial roles in negative regulation of skeletal muscle mass [1]. Similar to certain other TGF-β family members, myostatin is synthesized as a precursor, dimeric protein consisting of an N-terminal prodomain and C-terminal mature domain (ligand) [2,3]. After processing by furin-like proteases, the N-terminal prodomain noncovalently binds to the C-terminal ligand and forms an inactive latent complex to suppress its biological activities in circulation [3]. Upon cleavage of the prodomain by bone morphogenetic protein (BMP)-1/tolloid family of metalloproteinases, the ligand recruits and phosphorylates two distinct membrane serine/threonine receptors, termed type I and II, which in turn activate the intracellular effector molecule Mad homolog (Smad) 2 and Smad3, and subsequent Smad-responsive gene transcription [4,5]. Thus, the prodomain appears to be a crucial physiological inhibitor of the biological activity of myostatin [3]. The prodomain possesses the cleavage site for BMP-1/tolloid family of metalloproteinases [4], and the putative binding site for thrombospondin-1 (TSP-1), a major activator of the TGF-β1 ligand in recruitment of membrane receptors [6]. However, the regions critical for suppression of the myostatin signal have remained unknown.

Caveolin 3, a muscle-specific integral membrane protein, forms caveolae and functions as a scaffold protein by binding and regulating several signaling molecules such as Src tyrosine kinases, epidermal growth factor receptor, and G-proteins [7]. Heterozygous mutations in the *CAV3* gene give rise to limb-girdle muscular dystrophy (LGMD) 1C characterized by severe deficiency of caveolin 3 protein in muscle fibers [8]. We generated transgenic mice expressing Pro104Leu mutant caveolin 3 ($CAV3^{P104L}$). These LGMD1C model mice developed muscle atrophy with loss of caveolin 3, indicating a dominant-negative effect of the mutant caveolin 3 [9]. We found that activated type I receptor and subsequent intramuscular myostatin signaling in the caveolin 3-deficient atrophic muscles was ameliorated by genetic introduction of the full-length myostatin prodomain [10].

In the current study, we identified the inhibitory core in the prodomain required to suppress myostatin signaling by expressing various prodomain regions as Fc fusion proteins in assayed cells. We also explored the ability of the corresponding peptide to enhance myogenesis *in vitro* by addition to the culture medium of differentiating myoblasts and to increase muscle mass or ameliorate muscle atrophy *in vivo* by intramuscular injection into caveolin 3-deficient LGMD1C mice or their wild-type littermates. This study provides the basis for future peptide therapy of patients with muscular atrophy.

Materials and Methods

Plasmid vectors

To express various prodomain regions as Fc fusion proteins, the cDNA of each prodomain region was amplified by RT-PCR from human skeletal muscle mRNA and subcloned into the pcDNA3-hFc vector that harbors the human IgG1 Fc region at the C-terminus [11]. For immunoprecipitation, RT-PCR products of the C-terminal FLAG-tagged inhibitory core of the

prodomain and C-terminal V5- or HA-tagged ligand or receptor were subcloned into the pCS2 + expression vector.

Luciferase assay

The pGL3-$(CAGA)_{12}$-luciferase reporter gene contains the Smad-binding sequence (CAGA) [12]. HEK293 human embryonic kidney cells (Riken-BRC, Wako, Saitama, Japan) and A204 human rhabdomyosarcoma cells (ATCC, Manassas, VA, USA) were grown in Dulbecco's modified Eagle's medium (DMEM) and McCoy 5a medium supplemented with 10% fetal bovine serum (FBS), respectively. Cells were seeded in 12-well plates at 24 h before transfection with the pGL3-$(CAGA)_{12}$-luciferase reporter gene, pCMV-β-gal, and either the empty vector (pcDNA3-hFc) or pcDNA3-hFc harboring various prodomain regions as human Fc fusion proteins. After 24 h, the medium was replaced with serum-free DMEM containing 10 ng/ml recombinant myostatin, 10 ng/ml recombinant growth and differentiation factor 11 (GDF11), 6 ng/ml recombinant TGF-β1, or 10 ng/ml recombinant activin A (R&D Systems, Minneapolis, MN, USA). After an additional 24 h of culture, the cells were processed and their luciferase activity was measured by a luciferase reporter assay system (Promega, Madison, WI, USA). All experiments were performed in triplicate, repeatedly at least twice. Values were normalized to β-galactosidase activity as described previously [10,13].

The expression of fusion proteins was confirmed by immunoblot analysis using a goat anti-human Fc antibody (Jackson ImmunoResearch Labs, West Grove, PA, USA).

Co-localization and co-immunoprecipitation assay

COS-7 monkey kidney cells (Riken-BRC) were co-transfected with expression vectors bearing the FLAG-tagged inhibitory core of the prodomain with the V5- or HA-tagged ligand or receptor. All transfections were carried out in triplicate and the experiment was performed at least twice. The cells were fixed, permeabilized, and stained with an anti-rabbit FLAG polyclonal antibody (F7425; Sigma-Aldrich, St. Louis, MO, USA) and anti-mouse V5 monoclonal antibody (mAb) (R960-25; Invitrogen, Carlsbad, CA, USA) or anti-mouse HA mAb (12CA5; Roche Diagnostics, Indianapolis, IN, USA) for 60 min. Then, the cells were incubated with a fluorescent anti-rabbit and anti-mouse IgG secondary antibody (Invitrogen). The stained cells were visualized and imaged using a confocal laser microscope (TCS SP2, Leica Microsystems, Buffalo Grove, IL, USA).

Whole cell extracts were prepared by incubation in lysis buffer (50 mM Tris-HCl, pH 7.4, 50 mM NaCl, 1% Triton X-100, and 100 mM octyl glucoside) with a proteinase inhibitor cocktail on ice for 30 min as described previously [10]. After centrifugation at 10,000 × *g* for 30 min, the supernatant was incubated with an anti-FLAG mAb (M2, Sigma-Aldrich), anti-V5 mAb, or anti-HA mAb agarose gel to obtain immunoprecipitants as described previously [10].

In vitro myogenic differentiation assay

C2C12 mouse myoblasts (Riken-BRC) expressing myostatin, GDF11, activin A, TGF-β1, or Pro104Leu mutant caveolin 3 were generated using a retroviral system as described previously [13,14]. Mononucleated C2C12 myoblasts grown in DMEM supplemented with 10% FBS were induced to differentiate into multinucleated myotubes in differentiation medium consisting of DMEM supplemented with 2% horse serum (HS). The cells were subjected to Wright-Giemsa post-staining to evaluate fusion indices as described previously [13]. For immunocytochemical analyses, the cells were fixed, permeabilized, and stained with antibodies against anti-myosin heavy chain (MY-32; Sigma-Aldrich), muscle creatine kinase-M (N-13, Santa Cruz Biotechnology, Santa Cruz, CA, USA), or myogenin (F5D, Santa Cruz Biotechnology), followed by an

Alexa 488-conjugated secondary antibody (Invitrogen). Cell lysates were size-fractionated by SDS-polyacrylamide gel electrophoresis and immunoblotted using MY-32. These infection experiments were carried out in triplicate, repeatedly twice.

Experimental animals

All animal experiments were approved by the Recombinant DNA Experiments Safety Committee (#13–04) and Animal Research Committee (#13–081) of Kawasaki Medical School. $CAV3^{P104L}$ and wild-type littermate mice were maintained (n = 5 per cage) at 22°C under a 12:12 h light/dark cycle with free access to water and standard laboratory food (CE-2, CLEA Japan Inc., Fuji, Shizuoka, Japan). The water and food intake of the mice was monitored daily, and their body weights were recorded weekly. Muscles were isolated following euthanasia under sevoflurane-induced anesthesia.

Intramuscular injection of a synthetic peptide

A peptide corresponding to the 29-amino acid inhibitory core (p29) of mouse myostatin was synthesized and purified to >95% as assessed by high-performance liquid chromatography (KNC Laboratories, Kobe, Hyogo, Japan). The peptide (5–20 nmol) was injected into the ipsilateral tibialis anterior (TA) muscle of male caveolin 3-deficient transgenic mice ($CAV3^{P104L}$) [8,9] or wild-type littermate mice aged 12 weeks (n = 10) under inhalational anesthesia with sevoflurane. The same amount of albumin was injected into the contralateral TA muscle as a control. The specific tetanic force of the isolated TA muscles from the mice was measured as described previously [13]. Peak grip strength (g) was measured with a grip strength meter (MK-380S, Muromachi, Bunkyou-ku, Tokyo, Japan). At 1 month after peptide injection, the TA muscles were isolated, and the tetanic force, single myofiber area (SMA), satellite cell number, phosphorylated (p)-Smad2 level, and $Cdkn1a^{p21}$ or $Cdkn2b^{p15}$ gene expression were measured as described previously [10,13]. Single myofibers were isolated from the TA muscles as described previously [13,15]. Isolated myofibers were fixed, permeabilized, and stained for a satellite cell marker, caveolin 1 (BD Transduction Laboratories, Lexington, KY, USA) [16]. Nuclei were counterstained with 4′, 6-diamidino-2 phenylindole (DAPI) provided in the mounting media (Vectashield, Vector laboratories, Burlingame, CA, USA). Myofiber type immunohistochemistry was performed using monoclonal antibodies (Developmental Studies Hybridoma Bank, Iowa, IA, USA) against type I (BA-D5), type IIA (SC-71), and type IIB (BF-F3) myosin heavy chains and appropriate Alexa 594-conjugated secondary antibodies (Invitrogen).

Statistical analysis

Statistical analyses were performed using one-way analysis of variance followed by Bonferroni's test. P-values of less than 0.05 were considered statistically significant.

Results

Identification of the inhibitory core of the myostatin prodomain

We designed a series of truncation and deletion constructs of the full-length human prodomain including 239 amino acid residues (^{24}N–K^{262}). We considered two known sites:, ^{54}EAIKIQILSKL^{64}, the putative binding site for TSP-1 [6], and ^{97}QRD^{99}, the cleavage site for BMP-1/tolloid family of metalloproteinases [4] (Fig 1A). Each construct was co-transfected with a TGF-β-sensitive Smad-responsive luciferase reporter gene into HEK293 human embryonic kidney cells. To evaluate *in vitro* myostatin activities, luciferase reporter assays were performed

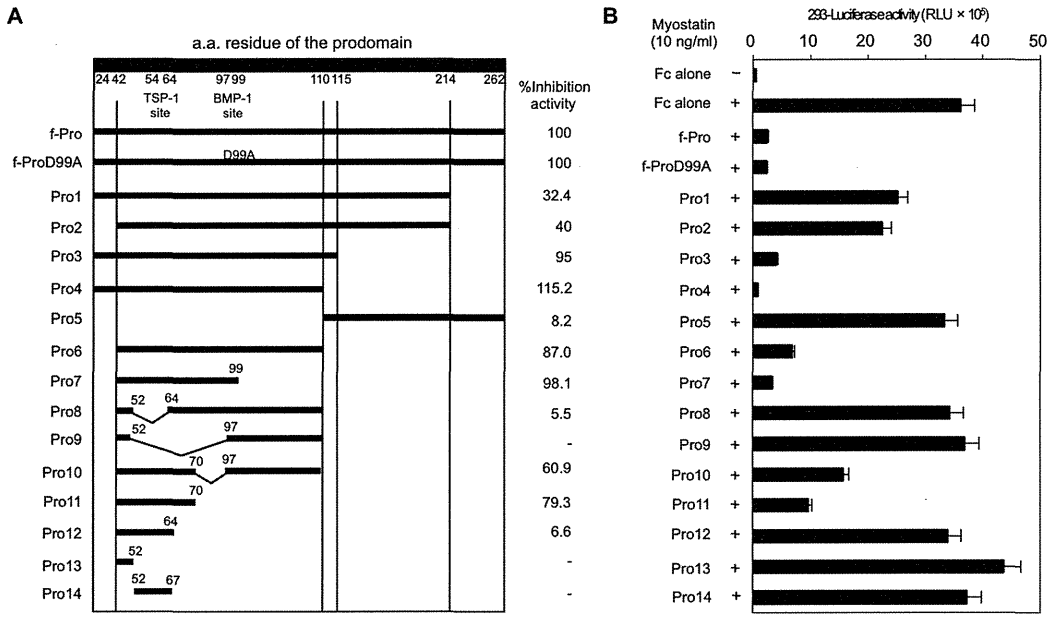

Fig 1. Identification of the inhibitory core of the myostatin prodomain. (**A**) Truncation and deletion constructs of human myostatin prodomain:human Fc fusion proteins (**left**). Percentage inhibitory effect of each construct on myostatin activity in comparison with the full-length prodomain (f-Pro, **right**). (**B**) Recombinant myostatin-induced transcriptional activity in HEK293 human embryonic kidney cells co-transfected with a pGL3-$(CAGA)_{12}$-luciferase reporter gene, pCMV-β-Gal, and various prodomain region:Fc fusion constructs. Values are the mean ± SD ($n = 6$). RLU, relative luminescence units.

doi:10.1371/journal.pone.0133713.g001

in triplicate, repeatedly at least twice. Stimulation of cells carrying an empty Fc vector with recombinant myostatin ligand significantly increased luciferase activity above the basal level (Fig 1B). Expression of the full-length prodomain:Fc fusion protein (f-Pro) resulted in a significant reduction of myostatin-induced transcriptional activity. Consistent with a previous report [4], a mutant (^{97}QAD^{99}) full-length prodomain:Fc fusion protein (f-ProD99A) was as effective at blocking myostatin-induced transcriptional activity as f-Pro. Additionally, f-ProD99A showed no proteolytic degradation products in immunoblot analysis (S1 Fig). We thus performed the following assays without considering the effect of cleavage by BMP-1/tolloid family of metalloproteinases.

Co-transfection of each truncated prodomain:Fc fusion protein suppressed luciferase activity in a region-specific manner (Fig 1). Compared with f-Pro, the N-terminal half of the prodomain (Pro4) showed a significantly increased capacity for inhibition of myostatin-induced transcriptional activity. In contrast, the C-terminal half of the prodomain (Pro5) lacked the inhibitory effect on myostatin-induced transcription. We thus assumed that the inhibitory core of the prodomain was located in the N-terminal half. We constructed expression vectors focusing on the N-terminal half including Pro6-14. As shown in Fig 1, Pro11, lacking the 19 N-terminal and 40 C-terminal amino acids of Pro4, showed 79% inhibitory activity compared with f-Pro. The inhibitory activity by Pro11 was higher than those by Pro8, Pro9, Pro10; neighborhood deletion constructs in consideration with the TSP-1 site and the BMP-1 site. Further deletion constructs from Pro11, including Pro12-14 also showed lower inhibitory effects on myostatin activity compared with Pro11. The inhibitory effect of Pro11 was consistent in A204 human rhabdomyosarcoma cells (S2 Fig). We conclude that Pro11 consisting of 29 amino acid residues is the inhibitory core of the myostatin prodomain.

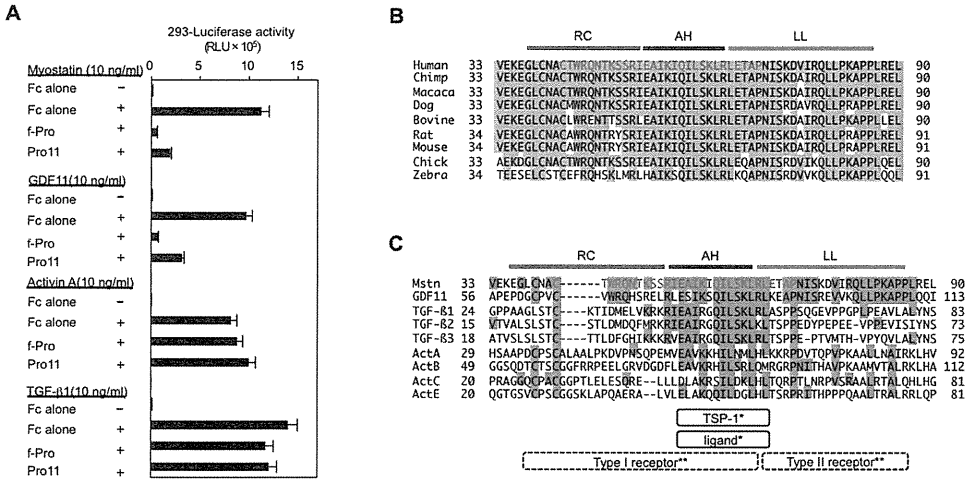

Fig 2. The identified inhibitory core of the myostatin prodomain specifically suppresses myostatin and its analog, GDF11, and includes an AH that is evolutionarily conserved among several other TGF-β family members. (**A**) The full-length myostatin prodomain (f-Pro) and its inhibitory core (Pro11) inhibited the transcriptional activities of myostatin and GDF11, but not of TGF-β1 or activin A, in HEK293 cells. (**B, C**) Sequence alignment of the prodomains of myostatin in nine species (**B**) and nine TGF-β family members (**C**). Red indicates the identified inhibitory core of the myostatin prodomain, consisting of 29 amino acids. The AH structure (blue) of the TGF-β1 prodomain has been shown to bind to both its ligand and TSP-1* [6,18]. Crystallographic analyses of TGF-β1 and its receptors have predicted that the random coiled structure (RC, green) and the AH are located closely to its type I receptor, whereas the latency lasso structure (LL, brown) is located close to its type II receptor** [19,20].

doi:10.1371/journal.pone.0133713.g002

The inhibitory core of the myostatin prodomain preferentially inhibits the biological activity of myostatin and its analog, GDF11

A previous study revealed that the full-length myostatin prodomain specifically suppresses myostatin and its analog, GDF11, but not activin [17]. We thus examined which TGF-β family members can be suppressed by the identified inhibitory core of the myostatin prodomain *in vitro*. As shown in Fig 2A, the inhibitory core (Pro11) inhibited not only myostatin, but also GDF11 to the same extent. In contrast, the activities of activin and TGF-β1 were not affected by the inhibitory core, suggesting certain specificity of the inhibitory core for suppression of TGF-β family members.

The inhibitory core of the prodomain suppresses myostatin activity by interacting with myostatin ligand and two distinct receptors

By creating a multiple sequence alignment from a protein BLAST, we found that the 29-amino acid inhibitory core in the human myostatin prodomain was well conserved not only in other species (Fig 2B), but also among other TGF-β family members (Fig 2C). Of note, a recent mutational analysis demonstrated that the corresponding region in the TGF-β1 prodomain includes an α-helix (AH) that binds to and suppresses the TGF-β1 ligand [18]. As shown in Fig 2C, the AH almost corresponds to the TSP-1 site. Importantly, more recent three-dimensional crystallographic analyses predicted that the inhibitory core of TGF-β1 was closely located to both type I and II receptors for TGF-β1 and the TGF-β1 ligand [19,20].

To explore the precise molecular mechanism by which the inhibitory core of the myostatin prodomain suppresses the biological activity of myostatin, we first examined whether the inhibitory core of the prodomain can interact with the type I and II receptors, and the myostatin

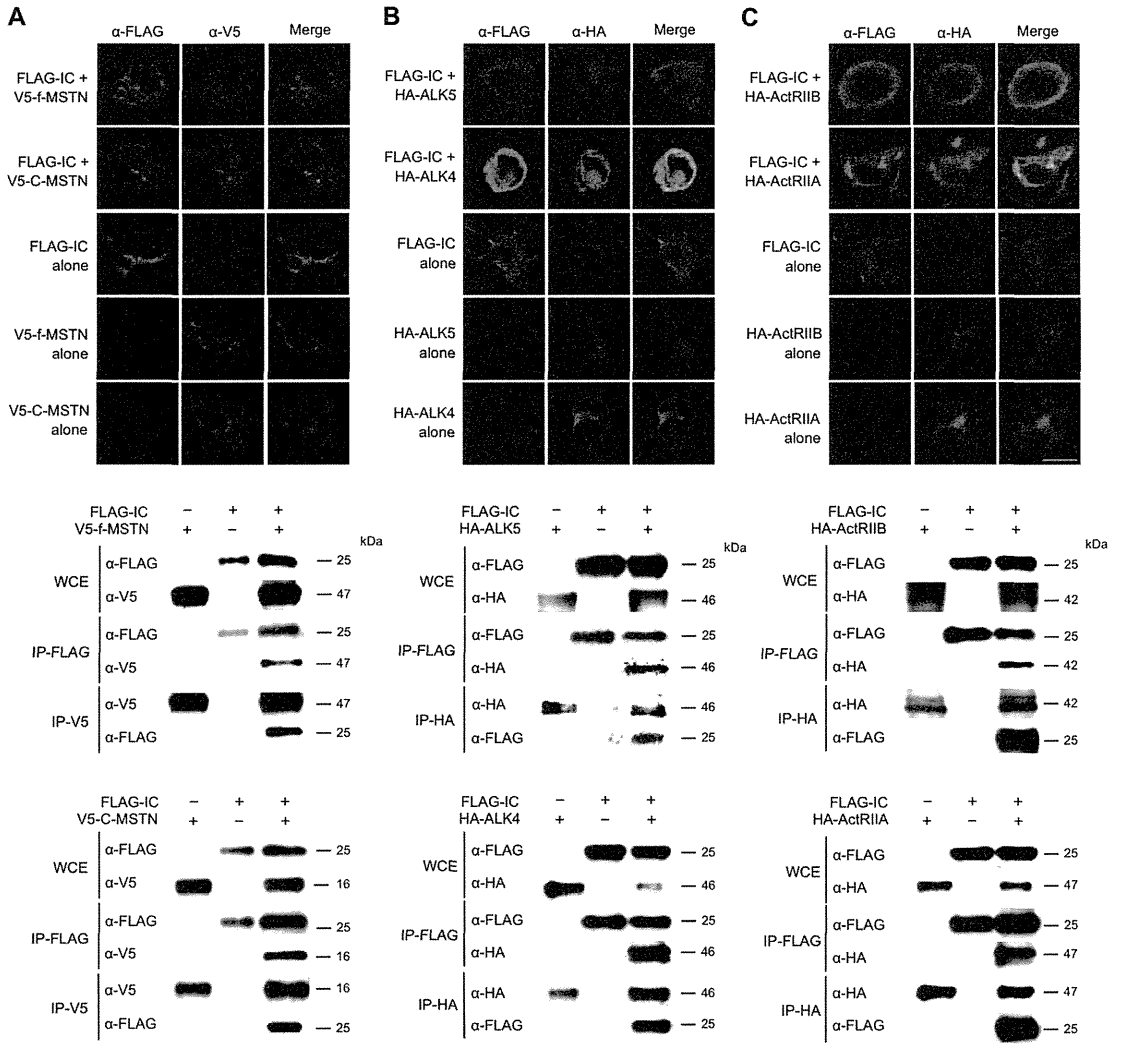

Fig 3. Interaction of the inhibitory core of myostatin with its ligand and receptors. Co-localization (**Upper**) and co-immunoprecipitation (**Lower**) of the inhibitory core (IC) of the myostatin prodomain and its ligand (**A**), its type I receptors (ALK4 and ALK5, **B**), and its type II receptors (ActRIIA and ActRIIB, **C**) in COS-7 embryonic kidney cells expressing FLAG-tagged IC and V5- or HA-tagged ligand or receptors. Scale bar, 20 μm. Whole cell extracts (WCE) were immunoprecipitated with anti-FLAG, anti-V5, or anti-HA agarose and then immunoblotted using anti-FLAG, anti-V5, or anti-HA antibodies, respectively.

doi:10.1371/journal.pone.0133713.g003

ligand. COS-7 monkey kidney cells were co-transfected with constructs harboring the C-terminal FLAG-tagged inhibitory core and V5-tagged full-myostatin (prodomain + ligand) or C-terminal mature myostatin (ligand). As expected, individually tagged proteins co-localized and co-immunoprecipitated with each other (Fig 3A). Similar results were observed for the FLAG-tagged inhibitory core and HA-tagged full-GDF11 (prodomain + ligand) or C-terminal mature GDF11 (ligand) (S3 Fig). To further explore the intriguing interactions of the inhibitory core with receptors, we co-transfected COS-7 cells with constructs harboring a FLAG-tagged inhibitory core and either HA-tagged type I (ALK5, ALK4) or type II (ActRIIB, ActRIIA) receptors [21]. Fig 3 shows co-localization and co-immunoprecipitation of the inhibitory core and each receptor (Fig 3B and 3C). These results suggest that the identified inhibitory core can

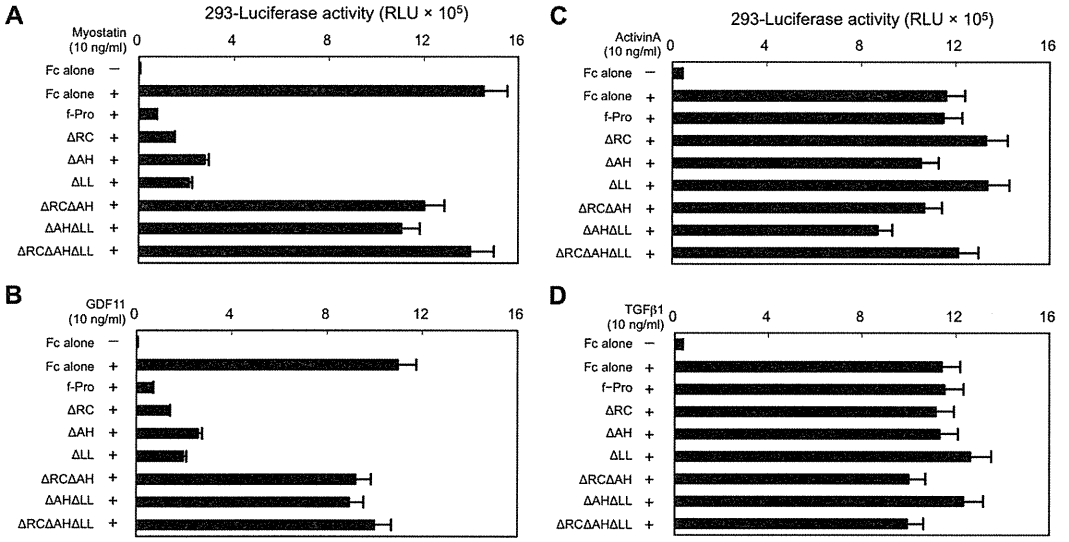

Fig 4. Three consecutive regions within the inhibitory core exhibit coordinated suppression of myostatin activity. Constructs (ΔRC, ΔAH, and ΔLL) with single deletions of the RC, AH, or LL regions of full-length myostatin (f-Pro) showed an inhibitory effect on the transcriptional activities of myostatin (**A**) and GDF11 (**B**), but not activin A (**C**) or TGF-β1 (**D**), in HEK293 cells. In contrast, combined deletion constructs (ΔRCΔAH, ΔAHΔLL, and ΔRCΔAHΔLL) had no inhibitory effect on myostatin (**A**) or GDF11 (**B**) activation in the HEK293-$(CAGA)_{12}$-luciferase system.

doi:10.1371/journal.pone.0133713.g004

interact not only with its ligand, but also the two receptors as previously predicted by TGF-β1 crystal structure analyses [19,20].

Next, we divided the 29-amino acid inhibitory core of the myostatin prodomain into three sections according to previous descriptions [18,19,20]: the N-terminal random coiled structure (RC, ^{42}CTWRQNTKSSRI^{53}), AH structure (AH, ^{54}EAIKIQILSKL^{64}), and C-terminal latency lasso structure (LL, ^{65}RLETAP^{70}). The AH has been shown to correspond to the binding site of the TGF-β1 prodomain for its ligand [18]. We constructed deletion constructs of RC, AH, or LL in the full-length prodomain and compared their inhibitory effects on myostatin signaling in HEK293 cells. As shown in Fig 4A, single deletion constructs (ΔRC, ΔAH, and ΔLL) significantly inhibited myostatin activity compared with f-Pro. However, combined deletion constructs (ΔRCΔAH, ΔAHΔLL, and ΔRCΔAHΔLL) lost their inhibitory activities, indicating that the three regions in the inhibitory core coordinately suppress myostatin activity by interacting with the receptors and ligand. Similar results were observed for GDF11 (Fig 4B), but not activin (Fig 4C) or TGF-β1 (Fig 4D).

A synthetic peptide corresponding to the inhibitory core, restores impaired myoblast differentiation induced by myostatin and GDF11, but not activin A or TGF-β1

To investigate the effect of the identified inhibitory core on *in vitro* myogenesis, we synthesized a peptide, termed p29, which corresponds to the 29-amino acid inhibitory core region of mouse myostatin (^{43}CAWRQNTRYSRIEAIKIQILSKLRLETAP^{71}). Using a retrovirus-mediated gene transfer system [13, 14], we established C2C12 mouse myoblasts expressing various TGF-β family members including myostatin, GDF11, activin A, and TGF-β1. Mononucleated C2C12 myoblasts differentiate into multinucleated myotubes. Myotubes were stained with antibodies against myosin heavy chain (MyHC), myogenin, and creatine kinase (CK) (Fig 5A). The levels

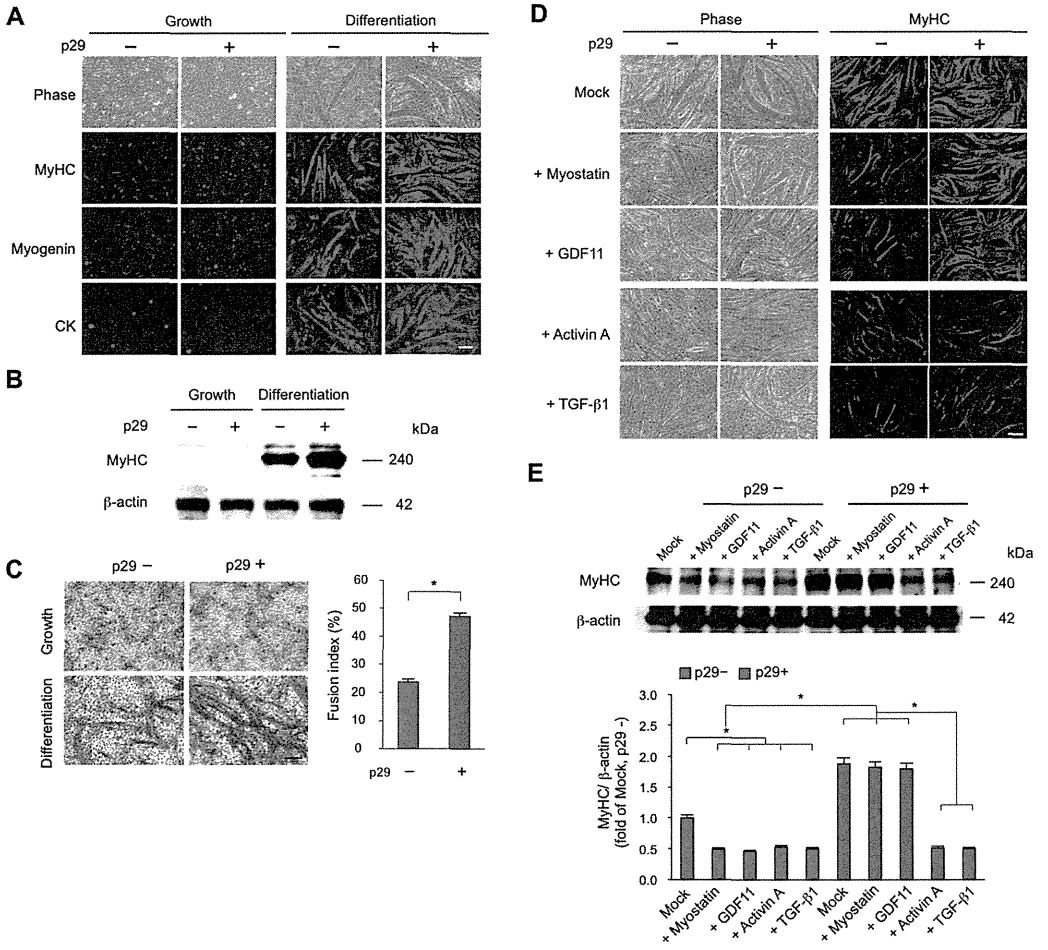

Fig 5. p29 enhances myogenesis suppressed by myostatin and GDF11, but not activin or TGF-β1. (**A**) C2C12 myoblasts were maintained in growth medium. Mononucleated myoblasts differentiate into multinucleated myotubes in differentiation medium with (+) or without (–) 1 μM p29 for 7 days. Phase-contrast and fluorescence images of cells stained for myotube markers MyHC, myogenin, and CK. Scale bar, 100 μm. (**B**) The protein analysis of MyHC in C2C12 cells expressing in growth or differentiation media with (+) or without (–) 1 μM p29. (**C**) Wright-Giemsa-stained C2C12 cells expressing an empty vector in growth or differentiation media with (+) or without (–) 1 μM p29 (**left**). Scale bar, 100 μm. Fusion indices were calculated in triplicate as the percentage of the total nuclei in myotubes/mm^2 (**right**). Values are the means ± SD ($n = 5$). *$P < 0.05$. (**D**) Phase-contrast (**left**) and fluorescence (**right**) images of MyHC in C2C12 myoblasts expressing the empty vector (mock), myostatin, GDF11, activin A, or TGF-β1 at 7 days after differentiation with (+) or without (–) 1 μM p29. Scale bar, 100 μm. (**E**) Immunoblot analysis of MyHC protein in C2C12 cells at 7 days after differentiation with (+) or without (–) 1 μM p29 (**upper**). Densitometric analysis (**lower**). Values are the mean ± SD fold increases compared with untreated C2C12 cells expressing the empty vector (mock) ($n = 5$). *$P < 0.05$.

doi:10.1371/journal.pone.0133713.g005

of MyHC protein were evaluated by immunoblot analysis (Fig 5B). We also quantified the fusion indices (Fig 5C). Addition of 1 μM p29 increased myotube formation and fusion Conversely, myotube formation was impaired in C2C12 myoblasts expressing TGF-β family members compared with controls expressing an empty vector (Fig 5D). Notably, p29 restored the impaired myotube formation induced by myostatin and GDF11, but not activin or TGF-β1. Consistently, p29 reversed the reduction in protein expression of MyHC in C2C12 myotubes induced by myostatin and GDF11, but not activin or TGF-β1 (Fig 5E). These findings indicate that p29 enhances myoblast differentiation by suppressing the activity of specific TGF-β family members including myostatin and its alalog GDF11 *in vitro*.

p29 ameliorates the impaired myogenesis caused by a LGMD1C-causing mutant caveolin 3 *in vitro*

We previously found that wild-type caveolin 3 binds to type I receptors (ALK4 and ALK5) and suppresses their activation, and that a LGMD1C-causing dominant-negative mutant caveolin 3 ($CAV3^{P104L}$) enhances type I receptor activation by expressing these molecules using plasmid vectors in COS7 cells [10]. We retrovirally expressed the LGMD1C-causing Pro104Leu dominant-negative mutant *CAV3* cDNA in C2C12 cells to explore the molecular significance of caveolin 3 in myoblast differentiation (Fig 6). Similar to the results of expressing TGF-β family members, myoblast differentiation was impaired in C2C12 myoblasts expressing the LGMD1C-causing mutant caveolin 3 compared with empty vector-expressing controls. p29 restored the impairment in myoblast fusion (Fig 6A) and myotube formation (Fig 6B and 6C) induced by the mutant caveolin 3. Together with our previous report [10], p29 could enhance myotube formation *in vitro* by suppressing the enhanced intracellular TGF-β signals caused by the dominant-negative mutation of caveolin 3.

p29 alleviates muscular atrophy and weakness in caveolin 3-deficient LGMD1C model mice

Before commencement of *in vivo* experiments, we assessed the effect of p29 on *in vitro* myostatin-induced transcriptional activity in the HEK293-$(CAGA)_{12}$-luciferase system. Consistent with our observations in co-transfection experiments, addition of p29 to the culture medium suppressed myostatin activity in a dose-dependent manner (Fig 7A). We next examined the effects of p29 in caveolin 3-deficient LGMD1C model mice ($CAV3^{P104L}$ Tg) with elevated intramuscular TGF-β signaling that leads to muscle atrophy [10]. We injected p29 into the ipsilateral TA muscle and the same amount of albumin simultaneously into the contralateral TA muscle as a control (20 nmol, $n = 10$). After 28 days, the mice were sacrificed and their TA muscles were isolated. The TA muscles injected with p29 were larger than those injected with albumin in both wild-type littermates and caveolin 3-deficient mice, suggesting an increase in muscle mass caused by p29 (Fig 7B). On the control side, the caveolin 3-deficient mice had significantly lighter muscles compared with the wild-type mice (35.8 ± 1.8 mg *vs.* 48.6 ± 2.4 mg, $n = 10$; $P < 0.05$; Fig 7C). p29 injection significantly increased muscle weights in both caveolin 3-deficient mice and wild-type littermates (caveolin 3-deficient: 20.6% increase compared with control injection; wild-type: 10.6% increase; Fig 7C). The muscle weight increases dose-dependently by local injection of p29 into the caveolin 3-deficient muscles ($n = 10$; Fig 7D).

We also evaluated the effect of p29 on muscle performance. The specific tetanic force of untreated TA muscles was significantly reduced in $CAV3^{P104L}$ Tg mice compared with wild-type mice ($n = 10$; Fig 7E). p29 injection increased the muscle-specific force in both $CAV3^{P104L}$ Tg and wild-type mice. Thus, a peptide that inhibited active myostatin restored muscle-specific force in caveolin 3-deficient atrophic muscle. However, tail vein injection of the same amount of p29 once a week from 6 to 11 weeks of age showed no effect on body weight gain or muscle grip strength in caveolin 3-deficient and wild-type mice ($n = 5$; S4 Fig).

Next, we examined hematoxylin and eosin-stained sections of the TA muscles from wild-type and caveolin 3-deficient mice treated with or without p29. $CAV3^{P104L}$ Tg mouse muscles exhibited a marked reduction in the myofiber size compared with wild-type mice ($n = 5$; Fig 8A, left). p29 treatment appeared to increase the myofiber size in both wild-type and $CAV3^{P104L}$ Tg mice. We also analyzed the single myofiber area (SMA) in each TA muscle. The SMA in TA muscles of p29-treated $CAV3^{P104L}$ Tg mice was significantly larger than that in untreated TA muscles (1226.6 ± 497.7 μm^2 *vs.* 752.4 ± 497.8 μm^2, $P < 0.05$; $n = 5$; Fig 8A, right). Consistently, the SMA of TA muscles in p29-treated wild-type mice was significantly

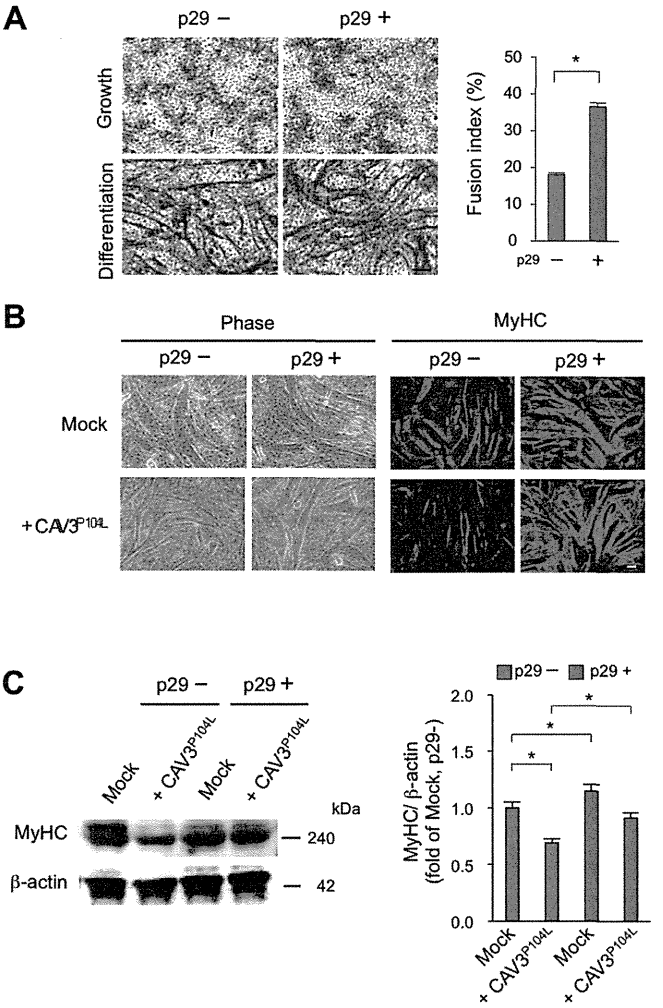

Fig 6. p29 restores the reduced myotube formation resulting from LGMD1C-causing mutant caveolin 3 ($CAV3^{P104L}$). (**A**) Wright-Giemsa-stained C2C12 cells expressing LGMD1C-causing Pro104Leu mutant caveolin 3 ($CAV3^{P104L}$) at 7 days after differentiation with (+) or without (–)1 μM p29 (**left**). Scale bar, 100 μm. Fusion indices of these cells following addition of 1 μM of p29 were calculated in triplicate as the percentage of the total nuclei in myotubes/mm^2 (**right**). Values are the means ± SD ($n = 5$). *$P < 0.05$. (**B**) (**C**) Phase-contrast (**left**) and fluorescence (**right**) images of MyHC in C2C12 myoblasts expressing the empty vector (mock) or Pro104Leu mutant caveolin 3 at 7 days after differentiation with (+) or without (–) 1 μM p29. Scale bar, 100 μm. (**C**) Immunoblot analysis of MyHC and β-actin in C2C12 cells expressing the empty vector (mock) or Pro104Leu mutant caveolin 3 ($CAV3^{P104L}$) at 7 days after differentiation with (+) or without (–) 1 μM p29 (**left**). Densitometric analysis (**right**). Values are mean ± SD fold increases compared with untreated C2C12 cells expressing the empty vector (mock) ($n = 5$). *$P < 0.05$.

doi:10.1371/journal.pone.0133713.g006

larger than that in p29-untreated wild-type mice (2102.7 ± 472.5 μm^2 *vs.* 1504.4 ± 353.4 μm^2, $n = 5$; $P < 0.05$; Fig 8A, right). Thus intramuscular p29 injection prevented myofiber hypotrophy in caveolin 3-deficient muscular dystrophy mice and induced postnatal myofiber hypertrophy in wild-type mice.

We further analyzed the change in fiber-type distribution by injecting p29 into TA muscles ($n = 5$; S5 Fig). We first observed that the superficial region of TA muscles consisted predominantly of fast glycolytic IIB fibers, while the deep region of TA muscles was composed of

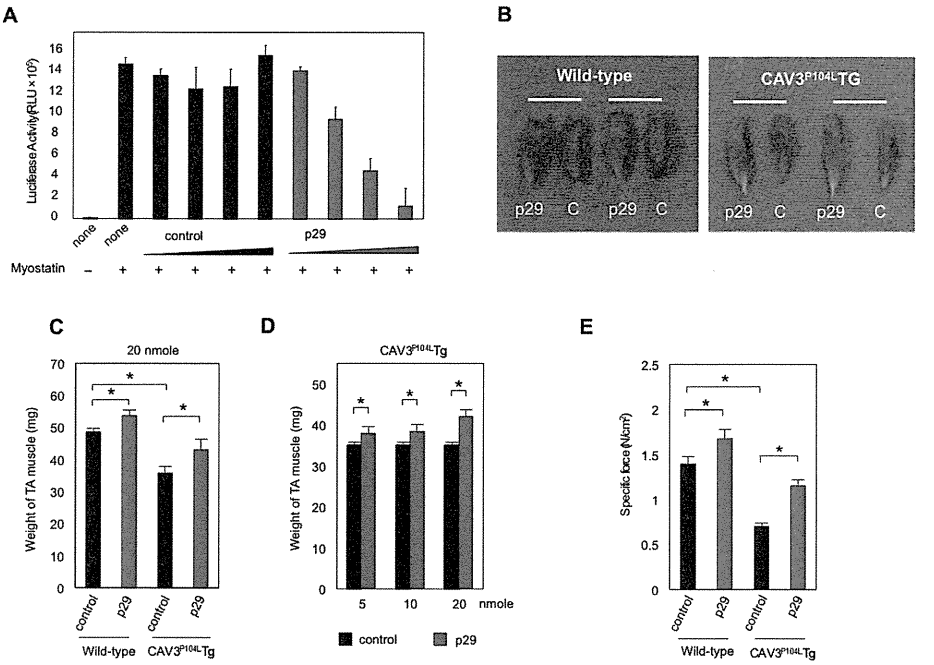

Fig 7. Intramuscular injection of p29 rescues muscle atrophy and weakness in caveolin 3-deficient LGMD1C model mice. (**A**) Effect of p29 on *in vitro* myostatin activity in the HEK293-$(CAGA)_{12}$-luciferase system. Cells were stimulated with 10-ng/ml myostatin and simultaneously exposed to increasing concentrations (2, 20, 200, or 2000 nM) of p29 or albumin (control). All experiments were performed triplicate, repeatedly twice. (**B**) Appearance of TA muscles at 28 days after local injection of p29 (20 nmol) or albumin (C, control) into the ipsilateral and contralateral TA muscles of wild-type and $CAV3^{P104L}$ Tg mice. (**C**) Weights of TA muscles injected with 20 nmol p29 or albumin in wild-type and $CAV3^{P104L}$ Tg mice ($n = 10$). *$P < 0.05$. (**D**) Weights of caveolin 3-deficient TA muscles injected with different amounts of p29 or albumin (**right**, $n = 10$). *$P < 0.05$. (**E**) Specific force of the TA muscle in wild-type (**left**) and $CAV3^{P104L}$ Tg (**right**) mice treated with p29 or albumin. *$P < 0.05$. Values are the means ± SD ($n = 10$).

doi:10.1371/journal.pone.0133713.g007

mainly IIB fibers but mixed with more abundant slow oxidative I and fast oxidative IIA fibers. In both regions, the p29 injection appeared to enlarge the size and number of IIB fibers, but not I or IIA fibers. We then measured the SMA of type IIB fibers in the deep region of TA muscles with or without p29 injection. Indeed, the SMA of type IIB fibers in p29-treated wild-type and $CAV3^{P104L}$ Tg mouse muscles was significantly larger than that in untreated mice (3271.0 ± 823.7 μm^2 *vs.* 2962.5 ± 476.3 μm^2 and 2858.5 ± 428.5 μm^2, *vs.* 1800.7 ± 224.9 μm^2, $n = 5$; $P < 0.05$; S6 Fig). Thus, p29 treatment changed the myofiber distribution to a faster glycolytic phenotype. This fiber-type change was consistent with previously reported myostatin-null mouse muscles [22].

Local injection of p29 increases the number of satellite cells and decreases intramuscular myostatin signaling

Satellite cells are resident stem cells between the myofiber and basal lamina in adult skeletal muscle [23]. We stained satellite cells with an anti-M-cadherin antibody in TA muscles from $CAV3^{P104L}$ Tg and wild-type mice ($n = 5$; Fig 8B, left). In p29-untreated muscles, the number of satellite cells per 100 myonuclei was significantly reduced in caveolin 3-deficient mice compared with wild-type mice ($n = 5$; Fig 8B, right). Conversely, p29 treatment increased the numbers of satellite cells in sections of caveolin 3-deficient and wild-type mouse muscles

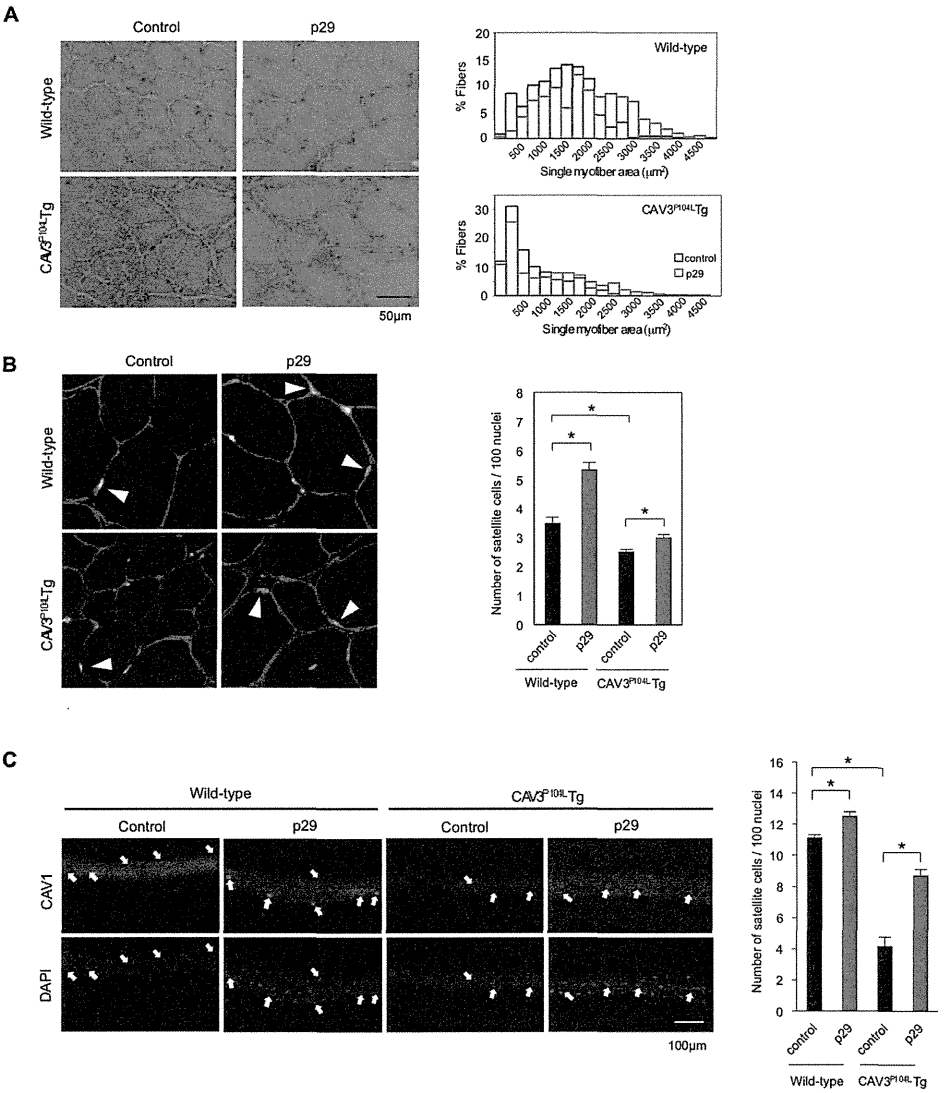

Fig 8. Local injection of p29 alleviates the reduction in myofiber size by restoration of the decreased numbers of satellite cells. (**A**) Histological analysis of TA muscles treated with p29 or albumin (control) in wild-type (**upper**) and CAV3^{P104L} (**lower**) mice. Scale bar, 50 μm (**left**). Distribution of SMAs in TA muscles of mice treated with p29 or albumin (**right**; $n = 7$; 250 myofibers were assessed in each mouse). (**B**) Immunohistochemical analysis of M-cadherin-positive satellite cells (green, arrows) in TA muscles of wild-type (**upper**) and CAV3^{P104L} (**lower**) mice (**left**) treated with p29 or albumin. Red indicates laminin α2 and gray indicates nuclei. Numbers of satellite cells per 100 myonuclei in TA muscles (**right**). One-thousand myonuclei were assessed in each muscle ($n = 7$). *$P < 0.05$. (**C**) Fluorescence images of satellite cells attached to single myofibers isolated from the TA muscles of wild-type (Wild) and CAV3^{P104L} mice treated with (+) or without (–) p29 (**left**). Mouse caveolin 1 (CAV1) was used as a marker of satellite cells (green). Nuclei were counterstained with DAPI (blue). The white arrow indicates (satellite cells). Quantification of the number of satellite cells attached to single myofibers (**right**). Numbers of satellite cells per 100 myonuclei (right). Data are expressed as the mean ± SD ($n = 5$). *$P < 0.05$.

doi:10.1371/journal.pone.0133713.g008

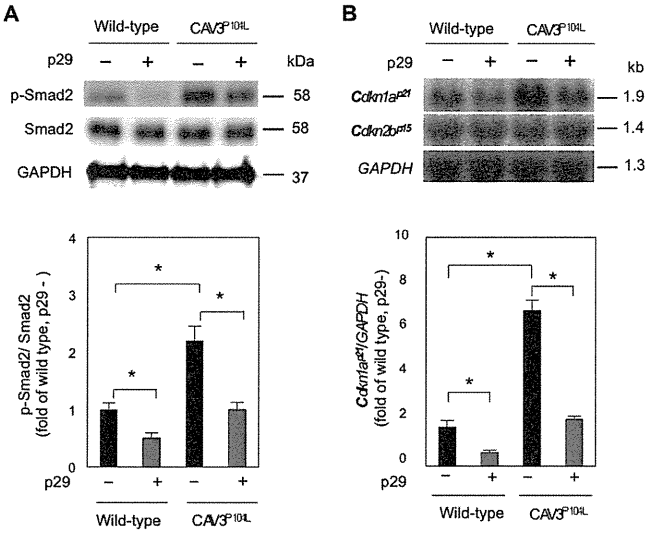

Fig 9. p29 inhibits activation of intramuscular myostatin signaling in caveolin 3-deficient LGMD1C model mice. Immunoblot ($n = 5$). (**A**) and northern blot ($n = 7$). (**B**) analyses of TA muscles treated with or without p29 (**upper**). Densitometric analyses (**lower**). Values are mean ± SD fold increases compared with untreated wild-type muscles. *$P < 0.05$.

doi:10.1371/journal.pone.0133713.g009

($n = 5$). We further stained satellite cells attached to isolated single myofibers from CAV3^{P104L} Tg and wild-type mice treated with or without p29 using an antibody against caveolin 1, another marker of satellite cells [16] ($n = 5$; Fig 8C, left). Isolated single myofiber from the CAV3^{P104L} Tg mice had a decreased number of caveolin 1-positive satellite cells compared with those from wild-type mice. Conversely, p29 injection restored the decreased number of satellite cells and myofiber size in CAV3^{P104L} Tg mice ($n = 5$; Fig 8C, right). Collectively, the synthetic peptide corresponding to the inhibitory core increased the number of resident stem cells *in vivo*.

To investigate the molecular mechanism by which p29 increases muscle mass, the levels of p-Smad2, the intracellular effector of myostatin, were analyzed in muscle homogenates ($n = 5$; Fig 9A). The amount of total Smad2 protein was comparable between wild-type and CAV3^{P104L} mice with or without p29 treatment. In contrast, the level of p-Smad2 was significantly higher in untreated muscles from CAV3^{P104L} mice. p29 treatment significantly reduced p-Smad2 levels in both wild-type and caveolin 3-deficient mice.

We previously found that cyclin-dependent kinase inhibitor p21 (*Cdkn1a*^{p21}) is a target gene of myostatin in mouse skeletal muscles [10,13]. To determine the effects of p29 on intramuscular myostatin signaling, the gene expression of *Cdkn1a*^{p21} was examined by northern blot analysis ($n = 7$; Fig 9B). *Cdkn1a*^{p21} expression was upregulated in p29-untreated caveolin 3-deficient muscles compared with untreated wild-type muscles, indicating activation of intramuscular myostatin signaling due to loss of caveolin 3. Notably, p29 injection downregulated *Cdkn1a*^{p21} expression in both wild-type and CAV3^{P104L} mice. In contrast, the expression of *Cdkn2b*^{p15}, which we have already shown to be unaltered by myostatin [10, 13], was not affected by p29 injection. These results are consistent with our previous *in vivo* findings indicating that genetic introduction of the full-length myostatin prodomain suppresses enhanced intramuscular myostatin signaling caused by caveolin 3 deficiency [10].

Discussion

In the current study, we revealed that the inhibitory core of the myostatin prodomain (^{42}CTWRQNTKSSRIEAIKIQILSKLRLETAP^{70}) resides near its N-terminus by expressing various prodomain regions as Fc fusion proteins in both HEK293 embryonic kidney cells, or A204 rhabdomyosarcoma cell. Our results are in contrast to those of a previous study in which a bacterially expressed GST-fused prodomain consisting of residues 42–98 had no inhibitory effect on *in vitro* myostatin-induced transcription [24]. The reason for this difference remains unknown, but co-expressed Fc fusion proteins might be more stable than purified GST-fusion proteins in the specific type of assay. Alternatively, peptides expressed in mammalian cells, but not prokaryotic cells, might achieve the properly folded state.

The identified inhibitory core of the myostatin prodomain includes an AH that is evolutionarily conserved among other TGF-β family members. Of note, a previous mutational analysis demonstrated that the AH in the TGF-β1 prodomain is required for both its ligand-binding and inhibitory capacities [18]. Recent three-dimensional crystallography analyses of TGF-β1 predicted that the neighboring portions of the AH (the N-terminal RC, and C-terminal LL) are located extremely close to their type I and type II receptors, and appear to shield the ligand from binding to its specific receptors [19, 20]. We demonstrated for the first time that the inhibitory core of the myostatin prodomain can interact with the type I and II receptors as well as the ligand by co-localization and co-immunoprecipitation experiments. We next found that combined deletion of portions of the inhibitory core (the RC, AH, or LL) in the full-length prodomain removes all inhibitory effects on myostatin activation. Moreover, we found that the myostatin inhibitory core specifically suppressed myostatin and its analog, GDF11, which shares identical type I and II receptors [25,26]. However, the myostatin inhibitory core did not suppress TGF-β1 or activin A, both of which have a similar AH structure but bind to different receptors [2, 5]. Additionally, the inhibitory core peptide (p29) enhanced restoration of the impaired myoblast differentiation induced by myostatin and GDF11, but not activin or TGF-β1. Consistent with our results, Thies et al. reported that the full-length myostatin prodomain suppresses *in vitro* transcriptional activities induced by myostatin and GDF11, but not activin A, in A204 cells [17]. Moreover, ligand-receptor binding of radiolabeled myostatin on the cell surface is dose-dependently suppressed by the full-length myostatin prodomain in L6 rat myoblast cells [17]. Taken together, our data suggest a novel concept that the identified inhibitory core of the myostatin prodomain has both binding and inhibitory effects on its ligand by coordinate interactions with type I and II membrane receptors. As observed in other crystal structure studies [27–29], the corresponding inhibitory core in the prodomain of certain TGF-βs are likely to co-locate approximately with its receptors, thus functioning to prevent an individual ligand from binding their two specific receptors on the cell surface.

Intramuscular injection of p29 increased muscle mass and strength by increasing the number of muscle precursor satellite cells in wild-type mice. Consistent with the *in vitro* results indicating that p29 reversed the impaired myogenic differentiation resulting from the LGMD-causing mutant caveolin 3, local injection of p29 alleviated muscle atrophy in TGF-β-activated muscles in LGMD1C model mice by restoration of enhanced TGF-β signaling *in vivo*. Thus, we have provided the first proof-of-concept of a synthetic peptide drug that blocks myostatin signaling to reverse muscle atrophy *in vivo*.

Several inhibitors that antagonize the activation of myostatin, a crucial negative regulator of muscle mass, have been developed recently to treat muscle-wasting disorders. These inhibitors include neutralizing antibodies against the myostatin ligand [30], its type II receptors [31], and type II decoy receptors [10,32], and a small molecule that inhibits type I receptors [13]. Compared with these nonphysiological blockers that target signal transduction molecules, the

inhibitory core peptide for the myostatin prodomain may be advantageous not only because it is a circulating physiological blocker of myostatin ligand in the inactive complex, but also because it disturbs ligand-receptor binding specifically on the cell surface. In the present study, intravenous injection of p29 failed to ameliorate muscle atrophy in TGF-β-activated LGMD1C model mice. The dosage of p29 for systemic administration could be insufficient to increase muscle mass. Alternatively, p29 peptide could be unstable against proteolysis when intravenously administered. Indeed, the bacterially expressed GST-fused prodomain peptide consisting of the N-terminal half is reported to be more unstable than that consisting of the C-terminal half [24]. We have recently revealed the precise peptide structure of the inhibitory core and its high affinity for the myostatin ligand [33]. Based on these structural data, further modifications of the degradation-competent amino acid architecture and the development of effective delivery methods to target skeletal muscle will advance rational and potent therapies incorporating synthetic myostatin-blocking peptides.

Supporting Information

S1 Fig. Immunoblot analysis of whole cell extracts using an anti-human Fc antibody (Upper) and the corresponding Ponceau S staining (lower). Left lane is a protein size standard.
(TIF)

S2 Fig. Luciferase activities in A204 rhabdomyosarcoma cells. (A) Truncation and deletion constructs of human myostatin prodomain:human Fc fusion proteins (left). Percentage inhibitory effect of each construct on myostatin activity in comparison with the full-length prodomain (f-Pro, right). (B) Recombinant myostatin-induced transcriptional activity in A204 cells co-transfected with a pGL3-$(CAGA)_{12}$-luciferase reporter gene, pCMV-β-Gal, and various prodomain region:Fc fusion constructs. Values are the mean ± SD (n = 6). RLU, relative luminescence units.
(TIF)

S3 Fig. Co-localization (A) and co-immunoprecipitation (B) of the inhibitory core (IC) of the myostatin prodomain with its analog, GDF11. (A) COS-7 cells expressing the FLAG-tagged IC of myostatin and HA-tagged GDF11 (prodomain+ligand, or ligand). Scale bar, 20 μm. (B) Whole cell extracts (WCE) were immunoprecipitated with anti-FLAG or anti-HA agarose, then immunoblotted using anti-FLAG or anti-HA antibodies, respectively.
(TIF)

S4 Fig. Growth curve and grip strength following systemic p29 injection. p29 (20 nmol) was injected intravenously once a week from 6 to 11 weeks of age into wild-type and caveolin 3-deficient mice (n = 5). Data are expressed as the mean ± SD (n = 5).
(TIF)

S5 Fig. Fiber type distribution of TA muscles treated with (+) or without (–) p29. Hematoxylin and eosin-, NADH-TR-, fast glycolytic type IIB MyHC-, fast oxidative type IIA MyHC-, and slow oxidative type MyH-stained sections showed the superficial and deep regions of TA muscles in wild-type (upper) and $CAV3^{P104L}$ Tg (lower) mice treated with (+) or without (–) p29. Fast (extensor digitorum longus, EDL) and slow (soleus) muscle sections from wild-type mice were used as a staining control. Scale bar, 50 μm.
(TIF)

S6 Fig. Histogram of the SMA of fast glycolytic type IIB fibers in the deep region of the TA muscles. The SMA in type IIB fast glycolytic fibers of wild-type (left) and $CAV3^{P1`4L}$ Tg (right)

mice treated with (red) or without (white) p29 (n = 5; 125 myofibers were assessed in each mouse).
(TIF)

Acknowledgments

We thank K. Tanda, E. Sugita, F. Uemura, H. Tsuruta, M. Kimura, M. Harada, N. Naoe, and T. Kenmotsu, M Tsuboi, K. Sakai (Department of Neurology, Kawasaki Medical School) for providing technical assistance.

Author Contributions

Conceived and designed the experiments: YO YS. Performed the experiments: K. Takayama TO MF YF TM. Analyzed the data: FI YH. Contributed reagents/materials/analysis tools: K. Tsuchida. Wrote the paper: YO SN HH YS.

References

1. McPherron AC, Lawler AM, Lee S-J (1997) Regulation of skeletal muscle mass in mice by a new TGF-beta superfamily member. Nature. 387: 83–90. PMID: 9139826
2. Massagué J (1998) TGF-beta signal transduction. Annu. Rev. Biochem. 67: 753–791. Review. PMID: 9759503
3. Hill JJ, Davies MV, Pearson AA, Wang JH, Hewick RM, Wolfman NM, et al. (2002) The myostatin propeptide and the follistatin-related gene are inhibitory binding proteins of myostatin in normal serum. J. Biol. Chem. 277: 40735–40741. PMID: 12194980
4. Wolfman NM, McPherron AC, Pappano WN, Davies MV, Song K, Tomkinson KN, et al. (2003) Activation of latent myostatin by the BMP-1/tolloid family of metalloproteinases. Proc. Natl. Acad. Sci. U S A. 100: 15842–15846. PMID: 14671324
5. Moustakas A, Souchelnytskyi S, Heldin C-H (2001) Smad regulation in TGF-beta signal transduction. J. Cell Sci. 114: 4359–4369. Review. PMID: 11792802
6. Crawford SE, Stellmach V, Murphy-Ullrich JE, Ribeiro SM, Lawler J, Hynes RO, et al. (1998) Thrombospondin-1 is a major activator of TGF-beta1 in vivo. Cell 93: 1159–1170. PMID: 9657149
7. Galbiat F, Razani B, Lisanti MP (2001) Emerging themes in lipid rafts and caveolae. Cell. 106: 403–411. Review. PMID: 11525727
8. Minetti C, Sotgia F, Bruno C, Scartezzini P, Broda P, Bado M, et al. (1998) Mutations in the caveolin-3 gene cause autosomal dominant limb-girdle muscular dystrophy. Nat. Genet. 18: 365–368. PMID: 9537420
9. Sunada Y, Ohi H, Hase A, Ohi H, Hosono T, Arata S, et al. (2001) Transgenic mice expressing mutant caveolin-3 show severe myopathy associated with increased nNOS activity. Hum. Mol. Genet. 10: 173–178. PMID: 11159934
10. Ohsawa Y, Hagiwara H, Nakatani M, Yasue A, Moriyama K, Murakami T, et al. (2006) Muscular atrophy of caveolin-3-deficient mice is rescued by myostatin inhibition. J. Clin. Invest. 116: 2924–2934. PMID: 17039257
11. Aruffo A, Stamenkovic I, Melnick M, Underhill CB, Seed B (1990) CD44 is the principal cell surface receptor for hyaluronate. CD44 is the principal cell surface receptor for hyaluronate. Cell 61:1303–1313. PMID: 1694723
12. Jonk LJ, Itoh S, Heldin C-H, ten Dijke P, Kruijer W (1998) Identification and functional characterization of a Smad binding element (SBE) in the JunB promoter that acts as a transforming growth factor-beta, activin, and bone morphogenetic protein-inducible enhancer. J. Biol. Chem. 273: 21145–21152. PMID: 9694870
13. Ohsawa Y, Okada T, Nishimatsu S, Ishizaki M, Suga T, Fujino M, et al. (2012) An inhibitor of transforming growth factor beta type I receptor ameliorates muscle atrophy in a mouse model of caveolin 3-deficient muscular dystrophy. Lab. Invest. 92: 1100–1114. doi: 10.1038/labinvest.2012.78 PMID: 22584670
14. Kitamura T, Koshino Y, Shibata F, Oki T, Nakajima H, Nosaka T, et al. (2003) Retrovirus-mediated gene transfer and expression cloning: powerful tools in functional genomics. Exp. Hematol. 31: 1007–1014. PMID: 14585362

15. Partridge TA (1997) Tissue culture of skeletal muscle. (1997) Methods Mol. Biol. 75: 131–144. PMID: 9276265

16. Volonte D, Liu Y, Galbiati F (2005) The modulation of caveolin-1 expression controls satellite cell activation during muscle repair. FASEB J. 19: 237–239. PMID: 15545301

17. Thies RS, Chen T, Davies MV, Tomkinson KN, Pearson AA, Shakey QA, et al. (2001) GDF-8 propeptide binds to and antagonizes biological activity by inhibiting GDF-8 receptor binding. Growth Factors. 18: 251–259. PMID: 11519824

18. Walton KL, Makanji Y, Chen J, Wilce MC, Chan KL, Robertson DM, et al. (2010) Two distinct regions of latency-associated peptide coordinates stability of the latent transforming growth factor-β1 complex. J. Biol. Chem. 285: 17029–17037. doi: 10.1074/jbc.M110.110288 PMID: 20308061

19. Radaev S, Zou Z, Huang T, Lafer EM, Hinck AP, Sun PD (2010) Thernary complex of transforming growth factor-β1 revels isoform-specific ligand recognition and receptor recruitment in the superfamily. J. Biol. Chem. 285: 14806–14814. doi: 10.1074/jbc.M109.079921 PMID: 20207738

20. Shi M, Zhu J, Wang R, Chen X, Mi L, Walz T, et al. (2011) Latent TGF-β structure and activation. Nature. 474: 343–349. doi: 10.1038/nature10152 PMID: 21677751

21. Lee S-J, McPherron AC (2001) Regulation of myostatin activity and muscle growth. Proc. Natl. Acad. Sci. U S A. 98: 9306–9311. PMID: 11459935

22. Girgenrath S, Song K, Whittemore L-A (2005) Loss of myostatin expression alters fiber-type distribution and expression of myosin heavy chain isoforms in slow- and fast-type skeletal muscle. Muscle Nerve. 31: 34–40]. PMID: 15468312

23. Cerletti M, Shadrach JL, Jurga S, Sherwood R, Wagers AJ (2008) Regulation and function of skeltal muscle satellite cells. Cold Spring Harb. Symp. Quant. Biol. 73: 317–322. doi: 10.1101/sqb.2008.73.054 PMID: 19204065

24. Jiang MS, Liang LF, Wang S, Ratovitski T, Holmstrom J, Barker C, et al. (2004) Characterization and identification of the inhibitory domain of GDF-8 propeptide. Biochem Biophys Res Commun. 315: 525–531. PMID: 14975732

25. Oh SP, Yeo CY, Lee Y, Schrewe H, Whitman M, Li E (2002) Activin type IIA and IIB receptors mediate Gdf11 signaling in axial vertebral patterning. Genes Dev. 16: 2749–2754. PMID: 12414726

26. Andersson O, Reissmann E, Ibáñez CF (2006) Growth differentiation factor 11 signals through the transforming growth factor-beta receptor ALK5 to regionalize the anterior-posterior axis. EMBO Rep. 7: 831–837. PMID: 16845371

27. Keller S, Nickel J, Zhang JL, Sebald W, Mueller TD (2004) Molecular recognition of BMP-2 and BMP receptor IA. Nat. Struct. Mol. Biol. 11: 481–488. PMID: 15064755

28. Nickel J, Kotzsch A, Sebald W, Mueller TD (2005) A single residue of GDF-5 defines binding specificity to BMP receptor IB. J. Mol. Biol. 349: 933–947. PMID: 15890363

29. Kotzsch A, Nickel J, Seher A, Sebald W, Müller TD (2009) Crystal structure analysis reveals a spring-loaded latch as molecular mechanism for GDF-5-type I receptor specificity. EMBO. J. 828: 937–947.

30. Bogdanovich S, Krag TO, Barton ER, Morris LD, Whittemore LA, Ahima RS, et al. (2002) Functional improvement of dystrophic muscle by myostatin blockade. Nature. 420: 418–421. PMID: 12459784

31. Lach-Trifilieff E, Minetti GC, Sheppard K, Ibebunjo C, Feige JN, Hartmann S, et al. (2014) An antibody blocking activin type II receptors induces strong skeletal muscle hypertrophy and protects from atrophy. Mol. Cell. Biol. 34: 606–618. doi: 10.1128/MCB.01307-13 PMID: 24298022

32. Lee S-J, Reed LA, Davies MV, Girgenrath S, Goad ME, Tomkinson KN, et al. (2005) Regulation of muscle growth by multiple ligands signaling through activin type II receptors. Proc. Natl. Acad. Sci. U S A. 102: 18117–18122. PMID: 16330774

33. Takayama K, Noguchi Y, Aoki S, Takayama S, Yoshida M, Asari T, et al. (2015) Identification of the minimum peptide from mouse myostatin prodomain for human myostatin inhibition. J. Medicinal Chem. 58:1544–1549.

Neurocognitive Impairment in Corticosteroid-naive Patients with Active Systemic Lupus Erythematosus: A Prospective Study

Katsuji Nishimura, Masako Omori, Yasuhiro Katsumata, Eri Sato, Takahisa Gono, Yasushi Kawaguchi, Masayoshi Harigai, Masaru Mimura, Hisashi Yamanaka, and Jun Ishigooka

ABSTRACT. ***Objective.*** Neurocognitive impairment (NCI) has been intensively studied in patients with systemic lupus erythematosus (SLE). However, those studies have mostly included patients who were treated with corticosteroids, which may itself induce NCI. We investigated NCI in corticosteroid-naive people with SLE who did not exhibit any overt neuropsychiatric manifestations.

Methods. Forty-three inpatients with SLE who had no current or past neuropsychiatric history participated in the study. Patients and 30 healthy control subjects with similar demographic characteristics were given a 1-h battery of neuropsychological tests. NCI was defined as scores at least 2 SD below the mean of the healthy control group on at least 2 of the 7 neurocognitive domains. Results of clinical, laboratory, and neurologic tests were compared regarding the presence of NCI.

Results. NCI was identified in 12 patients (27.9%) with SLE and in 2 control subjects (6.7%). Patients with SLE showed a significant impairment compared with controls on tasks assessing immediate recall, complex attention/executive function, and psychomotor speed. We identified psychomotor speed (Digit Symbol Substitution Test) as the factor that best differentiated the 2 groups. Further, we identified the score of the SLE Disease Activity Index 2000 as an independent risk factor for NCI in patients with SLE.

Conclusion. We conclude that reduced psychomotor speed is an SLE-specific pattern of NCI. Verbal-memory deficits that have been reported in patients with SLE were not evident among patients who were corticosteroid-naive. Our results indicate that impaired psychomotor speed may be added to the symptoms of early SLE. (First Release Jan 15 2015; J Rheumatol 2015;42:441–8; doi:10.3899/jrheum.140659)

Key Indexing Terms:
SYSTEMIC LUPUS ERYTHEMATOSUS NEUROCOGNITIVE IMPAIRMENT
CORTICOSTEROIDS

Systemic lupus erythematosus (SLE) is a chronic autoimmune disease involving multiple systems that has primary and secondary effects on the central nervous system (CNS) and psychosocial well-being. Neuropsychiatric (NP) manifestations are common in patients with SLE. Among the 19 different NPSLE syndromes identified by the American College of Rheumatology (ACR)[1], neurocognitive impairment (NCI) is the most frequent and is accompanied by a decreased quality of life. However, despite its prevalence, the etiology, nature, course, and treatment of SLE-associated NCI remains elusive.

NCI has been reported in patients with SLE who have[2,3,4] and do not have[4,5,6] overt NP symptoms. These studies suggest that NCI may be residual in patients with previous CNS impairments or may serve as an early marker of CNS impairment in patients who have not shown NP symptoms. However, to date, the nature of SLE-associated NCI has been studied mainly in longterm patients. One study, which targeted patients with newly diagnosed SLE, concluded that depression was associated with worse function in several cognitive domains[7]. Because SLE is typically a disease that takes some time to diagnose, NCI as well as other physical symptoms may occur before its diagnosis.

The mechanisms underlying SLE-associated NCI remain unknown. Antiphospholipid antibodies (aPL) have been reported to be associated with NCI, and neuroimaging studies have demonstrated that damage to white matter tracts may be a factor related to NPSLE, including NCI[8]. SLE-associated NCI might result directly from SLE or have

From the Department of Psychiatry and Institute of Rheumatology, Tokyo Women's Medical University School of Medicine, Tokyo; Kanagawa Psychiatric Center, Yokohama; Department of Pharmacovigilance, Graduate School, Tokyo Medical and Dental University; Department of Neuropsychiatry, Keio University School of Medicine, Tokyo, Japan.

K. Nishimura, MD, PhD; J. Ishigooka, MD, PhD, Department of Psychiatry, Tokyo Women's Medical University School of Medicine; M. Omori, MD, Kanagawa Psychiatric Center; Y. Katsumata, MD, PhD; E. Sato, MD; T. Gono, MD, PhD; Y. Kawaguchi, MD, PhD; H. Yamanaka, MD, PhD, Institute of Rheumatology, Tokyo Women's Medical University; M. Harigai, MD, PhD, Department of Pharmacovigilance, Graduate School, Tokyo Medical and Dental University; M. Mimura, MD, PhD, Department of Neuropsychiatry, Keio University School of Medicine.

Address correspondence to Dr. K. Nishimura, Department of Psychiatry, Tokyo Women's Medical University School of Medicine, 8-1 Kawada-cho, Shinjuku-ku, Tokyo 162-8666, Japan. E-mail: nishimura.katsuji@twmu.ac.jp

Accepted for publication November 25, 2014.

the same origin as NCI in the non-SLE population (e.g., psychological or psychiatric disturbances, pain, fatigue, sleep disturbance, or medication such as corticosteroids), and perhaps is exacerbated by SLE[8].

Specifically, corticosteroids are commonly used to treat SLE and are associated with NCI, whether patients have medical conditions[9] or are otherwise healthy[10]. The most extensively reported cognitive changes resulting from corticosteroid treatment involve declarative (verbal) memory, and occur during both short-term (high-dose)[9] and longterm (relatively low-dose)[11] therapies, reflecting a hippocampus-dependent process[12]. Further, even severe cognitive disorders such as dementia and delirium have been reported[13]. Corticosteroid-induced cognitive deficits have been thought to be related to dysfunctional hippocampal and frontal cortical neuroanatomic circuits[14]. Thus, corticosteroid therapy may affect the incidence and profile of NCI in patients with SLE. At the same time, although hippocampal atrophy in SLE has been demonstrated in 1 study, the use of corticosteroids could not be excluded as a factor that contributed to the memory deficits[15]. The 16/6 idiotype antibody of the human anti-DNA antibody has been reported to impair visual and spatial memory by causing hippocampal injury in mice[16]. Similarly, a recent study has indicated that anti-NMDA receptor subunit 2 (NR2) antibodies can cause neuronal death observed as hippocampal atrophy in patients with SLE[17], as previously demonstrated in mice with autoimmune disease[18].

In patients with SLE, however, the relationship between NCI and the use or dose of corticosteroids is controversial with negative[3,5,6,19,20] and positive[2,21] findings. McLaurin, *et al* reported that prednisone is associated with decreased cognitive functioning independent of SLE-associated disease activity[21]. In our present study we investigated whether SLE-associated NCI is related to corticosteroid treatment. We compared cognitive functioning between corticosteroid-naive patients with SLE and healthy control subjects, and studied psychological/health characteristics as well as neurological/immunological markers in SLE patients with or without NCI.

MATERIALS AND METHODS

Subjects. Subjects were Japanese patients who were admitted to the Institute of Rheumatology, Tokyo Women's Medical University Aoyama Hospital between 2000 and 2006 and who met all of the following criteria: (1) diagnosed with SLE based on the classification criteria of the ACR[22]; (2) no history of corticosteroid or other immunosuppressive therapy; (3) no physical condition such as high fever or general fatigue that would make them unable to participate in a psychiatric interview or complete the neuropsychological tests and questionnaires; (4) no history of major psychiatric disorders including substance abuse, except for adjustment disorder; and (5) no history of neurologic illness (e.g., persistent headache, strokes, seizures or movement disorders, head injury resulting in loss of consciousness, or any problems at birth). All patients were screened for current and previous major psychiatric conditions using the Structured Clinical Interview from the *Diagnostic and Statistical Manual of Mental Disorders*, fourth edition, Axis I Disorders, Non-patient Edition (with psychotic screening), Version 2.0 (SCID-I-NP)[23,24]. The study was approved by the ethics committee of Tokyo Women's Medical University and all participants gave informed written consent.

Of the 54 corticosteroid-naive patients with SLE who were admitted during the study period, 1 declined the invitation to participate, 2 were excluded based on the initial interview using SCID-I-NP (criterion 4), and 8 could not complete the neuropsychological tests (criterion 3). As a result, data from 43 patients were available for analysis. Demographic, clinical, and psychological characteristics for SLE and control groups can be seen in Table 1.

Controls. Thirty healthy controls were recruited from hospital staff and their relatives for neuropsychological testing. All controls were Japanese women with no history of major psychiatric disorder or neurologic illnesses as determined by the SCID-I-NP and neurologic history-related questions. This control group was similar in age and education to the SLE group (Table 1).

Neuropsychological assessment and data analysis. First, patients and controls completed the Mini-Mental State Examination (MMSE) to assess global cognitive functioning. Then a 1-h battery of neuropsychological tests was administered to both participant groups by a clinical psychometrist who was not aware of the clinical status and current medication of any patient. The neuropsychological tests included the Digit Span Test, Forward and Backward Test, Digit Symbol Substitution Test, Block Design Test, Similarities subsets of the Wechsler Adult Intelligence Scale-Revised (WAIS-R)[25]; Word Fluency Test (Animal Naming Test)[26]; Trail Making Test, Part A and B[26,27]; Rey Auditory-Verbal Learning Test (RAVLT)[26]; Wisconsin Card Sorting Test, Keio version (KWCST), and the Japanese version of the WCST[26,28]. In the Japanese version of the Trail Making Test, Part B, kana (Japanese phonograms) were used instead of Roman alphabet letters because performance has been shown to be similar[27]. These tests evaluated the following 7 cognitive domains: simple attention, complex attention/executive function, memory, visuospatial processing, language, reasoning/problem solving, and psychomotor speed. Table 2 shows the specific tests included in each domain and a short description of each test. These tests are consistent with the neuropsychological test battery recommended by the ad hoc committee of the ACR[1].

Because published normative data for the psychological tests used in this study lacked Japanese representation (except for the above-mentioned subsets of the WAIS-R), we used data from the healthy control group to estimate the population data. Scores on the Word Fluency Test and Trail Making Test Parts A and B were significantly different from those found in international normative data[29] (likely owing to linguistic differences or different formats), while scores on the RAVLT and KWCST were not different (data not shown). However, the scaled scores from an age-matched reference group (ages 25–34 yrs) were comparable to those of our healthy control group on several subsets of the Japanese WAIS-R (each of the 4 common subsets in the reference group: 10 ± 3; our controls: 9–12, with Digit Span = 9, Digit Symbol Substitution = 12, Block Design = 11, and Similarities = 11). This shows that our healthy controls had normal neurocognitive function.

Raw scores on the neuropsychological tests were converted to Z scores. Based on the criteria recommended by the Ad Hoc Committee on Lupus Response Criteria[30], performance on a single neuropsychological test was classified as impaired if the Z scores were at least 2 SD below the mean of the normal controls (rather than the recommended published normative data). If scores were impaired in at least 2 of the 7 neurocognitive domains, individuals were designated as cognitively impaired. When a domain comprised more than 1 test (e.g., complex attention/executive function), the domain was classified as impaired if at least 1 test showed significant impairment.

Psychological/health assessment. Following the neuropsychological session, both patients and controls were evaluated by the Profile of Mood States (POMS)[31]. POMS provides scores on 6 separate scales reflecting tension-anxiety, depression-dejection, anger-hostility, vigor, fatigue, and

Table 1. Demographic, clinical, and psychological characteristics of corticosteroid-naive patients with SLE versus healthy controls. Data are no./no. assessed (%) or median (interquartile range).

Characteristics	Patients with SLE, n = 43	Controls, n = 30	p
Demographics			
Age, yrs	28 (21–35)	25.5 (23.8–31.3)	0.822
Female	41/42 (97.6)	30/30 (100)	
Education, yrs	14 (12–15)	12 (12–15)	0.963
Clinical characteristics			
Disease duration, mos[a]	13 (5–36)	NA	
Time since SLE diagnosis, mos	0 (0–0)	NA	
Performance status[b]	0 (0–1)	NA	
Pain, VAS, mm	28 (8–57)	NA	
Fatigue, VAS, mm	26 (9–55)	NA	
SLEDAI-2K[c]	10 (8–16)	NA	
Profile of Mood State			
Tension-Anxiety	14 (8–20)	8.5 (7–15)	0.043[d]
Depression-Dejection	13 (6–22)	7 (4–17)	0.045[d]
Anger-Hostility	5 (3–14)	6 (4–8.3)	0.915
Vigor	8 (4–13)	10.5 (5.8–15.5)	0.098
Fatigue	10 (6–16)	8.5 (6–15)	0.590
Confusion	9 (6–13)	9 (6–12)	0.682
Total Mood Disturbance	44 (22–69)	30.5 (12–45)	0.074
Global cognitive functioning			
MMSE	30 (29–30)	30 (30–30)	0.017[d]

P values were determined by Fisher's exact test or Mann-Whitney U test. [a] Defined as the time between the SLE-attributable symptom onset and assessment. [b] Defined by Eastern Cooperative Oncology Group criteria. [c] Items included low complement in 37 patients (86.0%), increased DNA binding in 36 (83.7%), arthritis in 26 (60.5%), new rash in 20 (46.5%), leukopenia in 15 (34.9%), fever in 11 (23.2%), proteinuria in 9 (20.9%), hematuria in 8 (18.6%), urinary casts in 8 (18.6%), alopecia in 7 (16.3%), pleurisy in 5 (11.6%), pyuria in 5 (11.6%), thrombocytopenia in 4 (9.3%), mucosal ulcers in 3 (7.0%), pericarditis in 2 (4.7%), vasculitis in 1 (2.3%), myositis in 1 (2.3%), and visual disturbance in 1 (2.3%). The other SLEDAI-2K items (seizure, psychosis, organic brain syndrome, cranial nerve disorder, lupus headache, and cerebrovascular accident) were not found in any patient. [d] Significant variables. SLE: systemic lupus erythematosus; NA: not applicable; VAS: visual analog scale; SLEDAI-2K: SLE Disease Activity Index 2000; MMSE: Mini-Mental State Examination.

Table 2. Short description of neuropsychological test battery and examined cognitive domains.

Domain	Test	Short Description of Test
Simple attention	Digit Span, Forward*	Repeating random number sequences forward.
Complex attention/ executive function	Trail Making Test, Part B	Drawing lines to connect circles, alternating between numbered and lettered circles consecutively as quickly as possible.
	Digit Span, Backward*	Repeating random number sequences backward.
	Wisconsin Card Sorting Test, Keio version (KWCST)	Placing cards one by one under 4 stimulus cards, according to a principle that the subject must deduce from the pattern of the examiner's responses to the subject's placement of the card. Two sessions, each of which is composed of 48 trials.
Memory	Rey Auditory-Verbal Learning Test	Immediate recall trials after each of 5 repeated oral presentations of a 15-word list. Delayed recall trial after 20 min, followed by recognition of the 15 items among 15 distractor words.
Visual-spatial processing	Block Design*	Using 4 or 9 blocks (each block has 2 red, 2 white, and 2 red-white sides) to construct replicas of designs printed in a smaller scale.
Language	Animal Naming Test	Naming as many different animals as possible in 1 min.
Reasoning/problem solving	Similarities*	Describing how similar 2 words that represent common objects or concepts are.
Psychomotor speed	Trail Making Test, Part A	Drawing lines to connect consecutively numbered circles as quickly as possible.
	Digit Symbol Substitution*	Filling in blanks with symbols that are paired to numbers as quickly as possible for 90 s.

*Subsets of the Wechsler Adult Intelligence Scale-Revised.

confusion. The POMS Total Mood Disturbance score was derived by summing the scores on all the scales except vigor, which was subtracted out. The severity of depressive and anxious symptoms in patients was objectively evaluated by 1 of 2 psychiatrists (KN and MO) using the 17-item Hamilton Depression Rating Scale (HAMD-17) and the Hamilton Anxiety Rating Scale (HAMA). Sleep disturbance levels were derived by